Journal of Materials Chemistry B

Accepted Manuscript

ROYAL SOCIETY OF CHEMISTRY

www.rsc.org/materialsB

A rheumatoid arthritis magnetic resonance imaging contrast based on folic acid conjugated PEG-b-PAA@SPION

Yanqi Zhong,‡[ab] Fengying Dai,‡[a] Heng Deng,[ab] Meihong Du,[c] Xiaoning Zhang,*[d] Qingjun Liu*[c] and Xin Zhang*[a]

[a]National Key Laboratory of Biochemical Engineering, Institute of Process Engineering, Chinese Academy of Sciences, Beijing, 100190, PR China. Tel: +86 010 82544853; Fax: +86 010 82544853; E-mail address: xzhang@home.ipe.ac.cn

[b]University of Chinese Academy of Sciences, Beijing, 100049, PR China

[c]Beijing Center for Physical and Chemical Analysis, Beijing, 100089, PR China. Tel: +86 010 88487669; E-mail address: Liuqj@bjast.ac.cn

[d] School of Medicine,Tsinghua University, Beijing, 100084, China. Tel: +86 010 62785489; Fax: + 86 010 62785410; E-mail address: drugman@mail.tsinghua.edu.cn

1 Yanqi Zhong and Fengying Dai contributed equally to this work.

Abstract

Superparamagnetic iron oxide nanoparticle (SPION) offers unique properties for magnetic resonance imaging (MRI). Targeting imaging of rheumatoid arthritis *in vivo* requires a specific, magnetic sensitive and ultra-stable MRI contrast agent. In this study, SPION with preferable colloid stability and optimized size was obtained by using in situ polyol method with diblock copolymer PEG-b-PAA acting as surface ligand. Increasing the degree of polymerization (DP) of PAA from 18, 36 to 57 led to a decreasing size of iron oxide nanoparticles from 52 nm, 17 nm to 9 nm respectively. Folic acid was conjugated onto PEG-PAA_X@SPION as specific targeting molecule for activated macrophages in rheumatoid arthritis joint. To evaluate the stability and magnetic property of the particle, series of tests were conducted to evaluating and optimizing the nanoparticles. *In vitro* endocytosis experiments confirmed the better performance of folic acid conjugated SPION than non-folic acid modified SPION. *In vivo* MRI clearly demonstrated the significant signal diminishment of arthritis joint in antigen induced arthritis (AIA) rats by intravenous injection of the optimized

nanoparticle FA-PEG-b-PAA_{36}@SPION. These results indicated that the FA-PEG-b-PAA_{36}@SPION could serve as a promising candidate for MRI of rheumatoid arthritis.

1 Introduction

Rheumatoid arthritis (RA) is a permanent and incurable disease which causes high degree of morbidity.[1] Therefore, diagnosing the disease and assessing its severity is crucial for preventing the exacerbation of the disease. Among all the clinical imaging methods, magnetic resonance imaging (MRI) harbors a number of advantages including high spatial resolution and soft-tissue resolution over conventional radiography, which enable the characterization of structural damage of the joint in unprecedented detail and depth.[2] However, as one of the most commonly used T_1 weighted MR contrast agent, gadopentetate dimeglumine (Magnevist) shows some limitations in distinguishing normal and arthritic joint and failed to faithfully recapitulate all the facets of the arthritic joints including the degree of inflammatorycell recruitment.[3]

SPION contrast agent can pass through microvascular, be endocytosed by macrophages and serve as a molecule imaging agent to contrast and characterize the structure of joint.[3] In the past few years, many researchers were focusing on using SPION as MRI contrast agents for RA imaging.[4, 5] Hydrophobic nanoparticles produced by high-temperature thermo-decomposition reaction possess excellent magnetic sensitivity. However, hydrophobic nanoparticles need further modifications to transfer into water phase, which may lead to physiological unstable or

aggregation.[6-8] Moreover, controlling the core size of the nanoparticles is indispensable since larger nanoparticles may be endocytosed by RES system, whereas smaller nanoparticles suffer from weak magnetic sensitivity. Finally, without active-targeting molecule, SPION have shown limited MR signal enhancement.[8-10] Centering on these problems, this paper put forward an in situ polyol synthesized PEG-b-PAA@SPION contrast by thermo-decomposition reaction with high crystallinity and MR sensitivity. PEG coating was incorporated to offer good colloidal stability for magnetic iron oxide particles and proper length PAA block was used to control the core size of the nanoparticles.[11-13] Folic acid was conjugated onto PEG-b-PAA@SPION for its target binding to recruit and activate macrophages in synovium.[14] To reach the balance between stability and magnetic property of the particle, we have specifically designed a series of SPION with different core sizes. Various tests were conducted to evaluate and optimize the nanoparticles. With the selected nanoparticle PEG-b-PAA@SPION, MRI experiment exhibited enhanced performance in the diagnosis of RA *in vivo*.

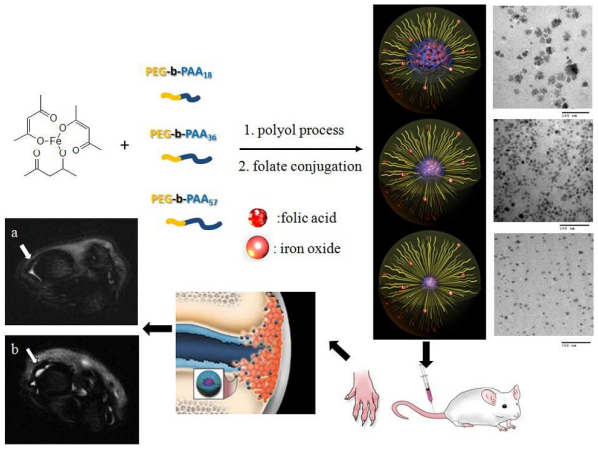

Scheme 1 Schematic representation of PEG-b-PAA$_x$@SPION synthesis with different core sizes

and evaluation of the optimized nanoparticle for enhanced magnetic resonance imaging of rheumatoid arthritis. Iron oxide cores were imaged to be red small balls in the scheme. PEG chains (yellow colored lines) were coated on the outer shell of the nanoparticle while PAA chains (blue colored lines) were firmly attached to the surface of the core. Folic acid molecules were represented as red small balls which were conjugated on the end of PEG molecules.

2 Experimental Section

2.1 Materials

HO-PEG-OH (M_w = 2000), iron(III) acetylacetonate ($Fe(acca)_3$) , tert-butyl acrylate, folic acid (FA), dicyclohexylcarbodiimide (DCC), 4-dimethylamiopyridine (DMAP), triethylene glycol (TREG) and trifluoroacetic acid (TFA) were purchased from Aladdin Reagent (shanghai,China). 2-Bromoisobutyryl bromide (98%), copper bromide (CuBr, 98%), *N, N, N′, N′, N″*-pentamethyldiethylenetriamine (PMDETA, 99%) and triethylamine (TEA, ≥99%) were purchased from Sigma-Aldrich (St. Louis, Missouri). All the reagents were analytical grade and used without further purification. High-purity water (Milli-Q Integral) with a conductivity of 18 MΩ/cm was used for the preparation of all aqueous solutions.

2.2 Synthesis of HO-PEG-Br

PEG-b-PAA_x diblock copolymers were synthesized by atom transfer radical polymerization (ATRP). Macroinitiator HO-PEG-Br was first synthesized by the reaction of HO-PEG-OH and 2-bromoisobutyryl bromide.[15] In brief, 10 g HO-PEG-OH and 0.505 g triethylamine were dissolved in 20 mL anhydrous dichloromethane, and then 1.15 g 2-bromoisobutyryl bromide dissolved in anhydrous

dichloromethane was added dropwise with gentle stirring at 0 °C. The solution was warmed to room temperature and stirred for 48 h. The mixture was washed three times with saturated sodium chloride solution containing a few drops of concentrated hydrochloric acid and then precipitated in cold diethyl ether.

2.3 Synthesis of PEG-PAA$_x$

HO-PEG-Br (1 equiv) was dissolved in a mixed solvent of 2-butanone and isopropanol (7:3), and then PMDETA (1.1 equiv), Cu(I)Br (1.1 equiv), monomers (5-100 equiv) were added. The mixture was degassed with nitrogen for 30 minutes and reacted at 50 °C for 24 hours. By controlling the different ratios of tBA monomer and macroinitiator HO-PEG-Br, PEG-b-PAA$_x$ with different tBA chain lengths were obtained. Specifically, PEG-b-PtBA$_{57}$, PEG-b-PtBA$_{36}$ and PEG-b-PtBA$_{18}$ were polymerized by initiator/monomer ratio of 100:1, 60:1 and 30:1, respectively. The mixture was filtered through an alumina column to remove copper and dialyzed against deionized water to remove residual tBA monomer and then lyophilized to obtain a white powder. The obtained PEG-b-PAA$_x$ was hydrolyzed in the solution of trifluoroacetic acid and dichloromethane (1:1) for 24 h. Residual TFA and dichloromethane were removed by rotary evaporation and a light yellow sticky product was obtained.

2.4 Synthesis of PEG-b-PAA$_x$@SPION

The synthesis was conducted as follows: 1.0 g PEG-b-PAA$_x$ was dissolved in 25 mL triethylene glycol in 100 °C. 1.0 g Fe (acac)$_3$ was added after the polymer was completely dissolved. The mixture was heated to 190 °C for 30 minutes. Afterwards

the solution was refluxed at 290 ℃ under a blanket of nitrogen for 30 minutes. The black product was then dialyzed against deionized water for 2 days and separated *via* centrifugation of 15000 rpm.

2.5 Conjugation of folic acid

The conjugation of folic acid was achieved *via* DCC/DMAP reaction. Folic acid (1 equiv) and DCC (1 equiv) were add to anhydrous DMSO and stirred overnight. PEG-PAA@SPION (1 equiv of HO-PEG-PAA_x) and DMAP (0.1 equiv) were then added. The solution was stirred for 24 h, and nanoparticles were separated *via* centrifugation of 15000 rpm.

2.6 Stability of PEG-PAA_x@SPION and FA-PEG-PAA_x@SPION

The stability test of PEG-b-PAA_x@SPION and FA-PEG-b-PAA_x@SPION was conducted by measuring the hydrodynamic diameter of nanoparticles dispersed into DMEM cell culture medium (10% FBS) for different periods of time (0, 12, 24, 48 and 72 hours). Hydrodynamic diameter was measured by dynamic light scattering (DLS) following the previous report.[16] Triple measurements of number-weighted mean size were performed.

2.7 Characterizations

The structure of PEG-b-PAA_x was examined by NMR (Bruker Avance 600 MHz, Bruker AXS Inc., Madison, Wisconsin). Hydrodynamic size and size distribution of the particles were measured by dynamic light scattering using a Malvern Zetasizer nano ZS apparatus (Malvern Instruments, Malvern, United Kingdom). The morphology of PEG-b-PAA_x@SPION was observed by transmission electron

microscopy (TEM, JEOL 2100F) at 120 kV. Thermogravimetric analysis (TGA) was performed using a TG-209-F3 thermogravimetric analyzer (Netzsch Instruments, Germany) with a heating rate of 10 °C /min from 30 to 800 °C in N_2 atmosphere. Magnetic measurements were carried out at room temperature using a MPMS XL-7 Quantum Design SQUID magnetometer (Quantum Design, America, San Diego) with the H magnetic intensity ranging from -1×10^4 to 1×10^4. UV vis spectrophotometry measurements were performed on TU-1810 ultraviolet and visible spectrophotometer (Persee, China) with a wavelength range from 250 nm to 800 nm. Surface compositions of the nanoparticles were analyzed *via* X-ray photoelectron spectroscopy (XPS) on a Thermo Escalab 250Xi (Thermo, America) with a monochromatized Al Kα X-ray source. The samples were mounted on the standard sample studs using double-sided adhesive tapes. Reference for binding energies (BEs) was 284.8 eV (C 1s hydrocarbon peak). NMR relaxometry of PEG-b-PAA_x@SPION was measured by a NMR spectrometer (Minispec, mq60, Bruker, Germany). Nanoparticles were dispersed in water with iron concentrations from 0.01 to 10 mM. Carr-Purcell-Meiboom-Gill pulse sequence was used to measure T_2 relaxation time, and the slope of linear fit of $1/T_2$ versus iron concentrations is the r_2 value of SPION.

2.8 Cell culture and Prussian blue staining of cells

RAW 264.7 cell was purchased from Fuxiang biotech company, China, Shanghai. Cells were cultured in 12-well polystyrene dishes at 37 °C in a humidified atmosphere of 5% CO_2 and 95% air in DMEM high glucose medium containing 10% FBS and supplemented with penicillin (100 units/mL) and streptomycin (100 units/mL).

Activation of RAW264.7 cells was conducted as described before.[17] RAW 264.7 cells were plated in 24-well plate at density of 2×10^4 per well, and cytokines IFN-γ and TNF-α were added to cell culture medium with the final concentration of 200 U/mL and 100 U/mL for 24 hours. Concentration and time dependent RAW 264.7 cells uptake of FA-PEG-b-PAA_x@SPION were conducted by co-culturing SPION with RAW264.7 cells at different time or concentration. Once the incubation was ended, cells were washed with PBS for three times and fixed with 500 μL paraformaldehyde (4%) for 30 minutes, and then incubated for 30 minutes at 37 ℃ with 500 μL Prussian blue solution containing 10% hydrochloride and 20% potassium ferrocyanide (II) trihydrate.

2.9 Ferrozine assay

Iron concentrations were measured using the ferrozine assay. Cells were washed three times with PBS after incubation. 250 μL reagent A (4.5% $KMnO_4$ and 1.2 M HCl mixed at equal volumes) was added and mixed for 1 hour. After that 50 μL reagent B (6.5 mM ferrozine, 13.1 mM neocuproine, 2 M ascorbic acid and 5 M ammoniumacetate) was added. Absorbance of samples was tested at 570 nm using a BioRadmicroplate reader and standard curve was prepared with ferrous ethylenediammonium sulphate in 0.01 M HCl, ranging from 0 to 60 mg/mL.

2.10 SPION enhanced MRI of Antigen-Induced Arthritis

All procedures involving experimental animals were performed in accordance with the Guide for the Care and Use of Laboratory Animals (NIH publication no. 86-23, revised 1985). Lewis rats were sensitized by intradermal injection at back feet with

100 μL complete Freund's adjuvant mixed and completely emulsified with physiological saline. Joint inflammation was assessed by measuring the diameter of the ankle joint. Inflammation of the four paws was graded from 0 to 4 according previous literature.[18] After 14 days, animals were all graded to validate the AIA model for further use. 21 days after complete Freund's adjuvant injection, animals were intravenous injected of PEG-b-PAA_{36}@SPION or FA-PEG-b-PAA_{36}@SPION at a dose of 5 mg/kg. The infected right hind ankle was imaged with a 7-T Bruker (Bruker Medical Systems, Germany). T_2-weighted imaging sequence was applied and a transverse section orientation was selected. Signal intensity was quantified through the signal intensity ratio of surrounding water proton / the arrowhead indicated area. The parameters were as follows: TR = 3000, TE = 45, matrix = 256×256, field of view (FOV) = 3.0×3.0 cm^2, slice thickness = 1.00 mm and number of excitation (NEX) = 1.

2.11 Histopathology assessment

After the MRI, the animals were sacrificed. Main organs and ankle joints were harvested and fixed in 10% neutral buffered formalin for 24 hours, after that they were decalcified over night, and processed through a gradient of alcohols for paraffin embedding. For hematoxylin-eosin staining, slides were immersed in the stain, washed, and mounted in p-xylene-bis-pyridiniumbromide (VWR, Dorset, England) with obtained tissues section of 5 μm. For Prussian blue staining, slides were incubated with an equal mixture of fresh 2% hydrochloric acid and 2% potassium ferrocyanide for 30 minutes at room temperature. Afterwards, slides were washed and

counterstained with nuclear fast red.

3. Results and discussion

3.1 Preparation and characterization of PEG-b-PAA_x@SPION

The synthesis of the magnetite nanoparticles was carried out by reacting iron precursor, iron (III) acetylacetonate ($Fe(acac)_3$), with PEG-b-PAA_x at elevated temperature. Block copolymer of PEG-b-PAA_x in this reaction played a dual role in controlling the core size of iron oxide particles efficiently and enhancing colloidal stability of iron oxide particles in the physiological environment. Learning from the previous studies that an exceedingly long chain of PEG might have an adverse impact on r_2 relaxation, moderate length of PEG (M_w=2000) was adopted in our study.[19, 20] Three block copolymers of PEG-b-PAA_x with different chain length of PAA were synthesized *via* ATRP. The synthesis route of PEG-b-PAA_x coated SPION was shown in Scheme. 1.

Fig. 1 exhibited the ^1H NMR spectra of HO-PEG-Br, PEG-b-$PtBA_x$ and PEG-b-PAA_x block polymer. In macroinitiator HO-PEG-Br, feature signals of -CH_2-CH_2O- (δ = 3.68) and -C(CH_3)$_2$Br (δ = 1.98) appeared, which indicated the formation of OH-PEG-Br. The structure of PEG-b-$PtBA_x$ was confirmed by the feature peak of -C(CH_3)$_3$ (δ = 1.45), -C*H*-CH_2- (δ = 2.23) and -CH-CH_2- (δ = 1.86), which belonged to the PtBA block. After the copolymers were hydrolyzed by trifluoroacetic acid (TFA), peak of -C(CH_3)$_3$ disappeared and the two peaks at main chain -C*H*-CH_2- (δ = 2.31) and -CH-CH_2- (δ = 1.51) were slightly moved.[21, 22] DP (degree of polymerization) was calculated according to integral area ratio. For

instance, DP of PtBA was calculated to be 36 based on the integral area ratio of -CH_2-CH_2O- and -C(CH_3)$_3$, Fig. 1S exhibited ^{1}H NMR spectra of three kinds of PEG-b-PtBA$_x$. DP of PtBA could be calculated from the integral area ratio of -CH_2-CH_2O- and -C(CH_3)$_3$. By controlling the adding amount of tBA monomer, PEG-b-PtBA$_{18}$, PEG-b-PtBA$_{36}$ and PEG-b-PtBA$_{57}$ were synthesized.[23,24]

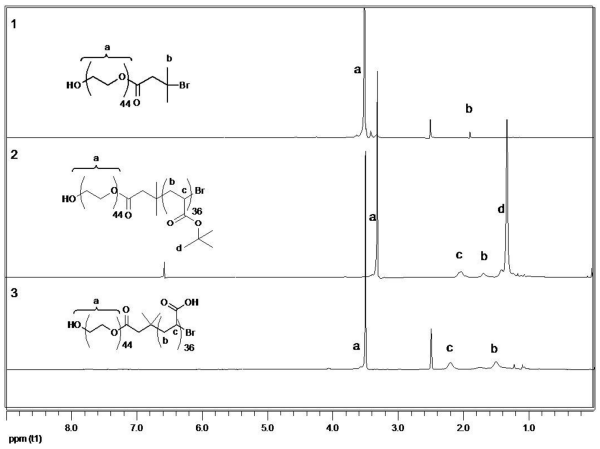

Fig. 1 ^{1}H NMR spectra of (1) HO-PEG-Br dissolved in DMSO-d6; (2) PEG-b-PtBA$_{36}$ dissolved in $CDCl_3$ and (3) PEG-b-PAA$_{36}$ dissolved in DMSO-d6.

3.2 Size and colloid stability of PEG-PAA$_x$@SPION

The size of iron oxide nanoparticles was confirmed by transmission electron microscopy and dynamic light scattering analysis in aqueous medium (Fig. 2 and Table 1). TEM observation result indicated that PEG-b-PAA$_{57}$@SPION and PEG-b-PAA$_{36}$@SPION presented similar mono-dispersed and spherical-like structures. The average core sizes of these two particles were 6.6±0.7 nm and 12.4±1.3 nm respectively, whereas PEG-b-PAA$_{18}$@SPION showed a larger core size of 36.6±9.3 nm. It might result from the inefficiency in controlling iron oxide crystal growing of the shorter chain length of PAA$_{18}$ and the structure of

PEG-b-PAA_{18}@SPION was largely consistent with recent report on polyol process synthesis of iron oxide nanoparticles.[25] Hydrodynamic diameters of PEG-b-PAA_{57}@SPION, PEG-b-PAA_{36}@SPION and PEG-b-PAA_{18}@SPION were 9.2±1.2 nm, 17.7±1.4 nm and 52.0±5.2 nm, respectively, which were in consistent with TEM results (Table 1).

Colloid stability was very important for the design of SPION as an MRI contrast agent. To assess the stability of SPION, the nanoparticles were incubated in DMEM cell culture medium containing 10% FBS and the hydrodynamic sizes were tested by DLS in different time (Fig. 3). PEG-b-PAA_{36}@SPION and PEG-b-PAA_{57}@SPION were stable and didn't have any significant change for 72 hours, whereas PEG-b-PAA_{18}@SPION tended to aggregate and gradually precipitate in the solution. The optimized magnetic particles PEG-b-PAA_{36}@SPION and PEG-b-PAA_{57}@SPION were selected for further arthritis MRI study.

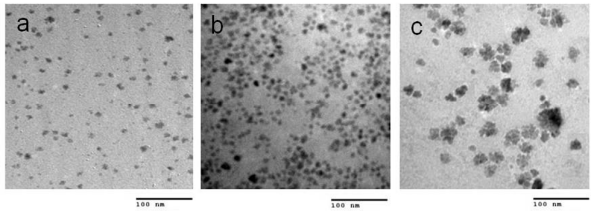

Fig. 2 TEM images of (a): PEG-b-PAA_{57}@SPION; (b) PEG-b-PAA_{36}@SPION and (c) PEG-b-PAA_{18}@SPION.

Table 1 Hydrodynamic size and core size of PEG-b-PAA_{57}@SPION, PEG-b-PAA_{36}@SPION and PEG-b-PAA_{18}@SPION.

Polymer coated nanoparticles	Core size (nm)	Hydrodynamic size (nm)
PEG-b-PAA_{57}@SPION	6.6±0.7	9.2±1.2

PEG-b-PAA_{36}@SPION	12.4±1.3	17.7±1.4
PEG-b-PAA_{18}@SPION	36.6±9.3	52.0±5.2

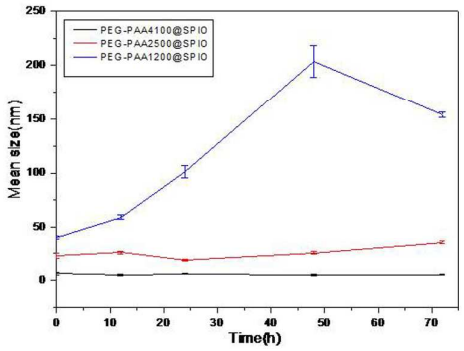

Fig. 3 Serum stability of PEG-b-PAA_x@SPION.

3.3 Synthesis of folic acid conjugated PEG-PAA_x@SPION

Macrophages played a major role in various stages of RA, as previous research has shown that MRI signal of normal synovium remained constant after intravenous administration of SPION since there were no activated macrophages in normal synovium.[26] Macrophages have been proven to be a biomarker for inflamed lesions assessment of RA. SPION MRI contrast agent targeting macrophages might have high sensitivity and specificity for the evaluation of RA. In this section, folic acid conjugated PEG-PAA_x@SPION for targeting MRI of rheumatoid arthritis was obtained by esterification reaction. The conjugation of folic acid and SPION was confirmed by XPS as seen in Fig. 4a and b. N1s peak was shown in wild-scan spectra of FA-PEG-b-PAA_{57}@SPION and FA-PEG-b-PAA_{36}@SPION, whereas no significant N1s peaks were found in the spectrum of PEG-b-PAA_{57}@SPION and PEG-b-PAA_{36}@SPION. C1s core-level spectra of PEG-b-PAA_{57}@SPION and PEG-b-PAA_{36}@SPION (Fig. 4 c and d) could both be curve-fitted with three peaks at

binding energies (BEs) of 284.6, 286.2, and 288.6 eV, which were attributed to C-C/C-H, C-O, and O=C-O bond, respectively.[27] By comparison, two new peaks at 285.6 and 287.8 eV in FA-PEG-b-PAA_{57}@SPION and FA-PEG-b-PAA_{36}@SPION (Fig. 4 e and f) were attributed to the peaks of C-N and O=C-N bonds, which belongs to the conjugated folic acid.[28] UV spectrophotometry method (Fig. 5) was also used to verify the existence of folic acid. The characteristic absorption peak of folic acid located at 280 nm was exhibited at the spectra of FA-PEG-b-PAA_{57}@SPION and FA-PEG-b-PAA_{36}@SPION,[29] while absent at the spectra of PEG-b-PAA_{57}@SPION and PEG-b-PAA_{36}@SPION. The UV-vis spectrophotometry feature of folic acid conjugated SPION was consistent with previous report on the chemical conjugation of FA.[30] The conjugation of FA onto the particles could be quantified by using a calibration curve of free FA (Fig. S3). The amount of conjugated FA was calculated to be 40.7 and 20.5 mg/(g·nanoparticles) for FA-PEG-b-PAA_{36}@SPION and FA-PEG-b-$PAA_{57,}$ respectively.

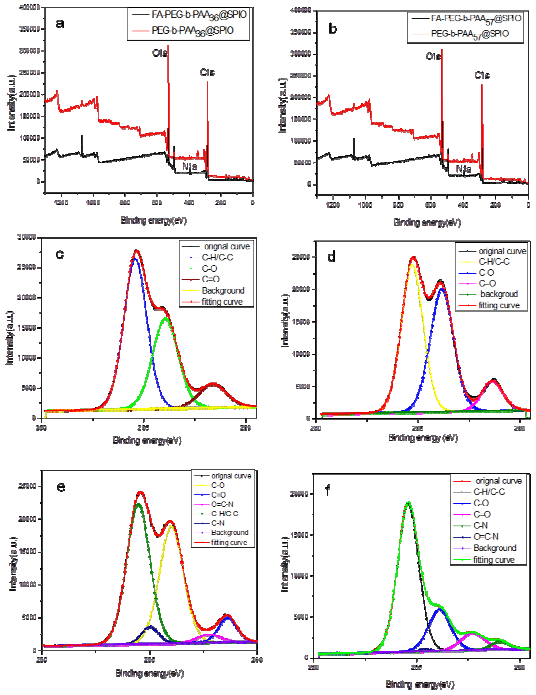

Fig. 4 XPS wild scan spectra of FA-PEG-b-PAA_{36}@SPION and FA-PEG-b-PAA_{57}@SPION (a and b); C1s core-level spectra of PEG-b-PAA_{36}@SPION (c); C1s core-level spectra of FA-PEG-b-PAA_{36}@SPION (e); C1s core-level spectra of PEG-b-PAA_{57}@SPION (d); C1s core-level spectra of FA-PEG-b-PAA_{57}@SPION (f).

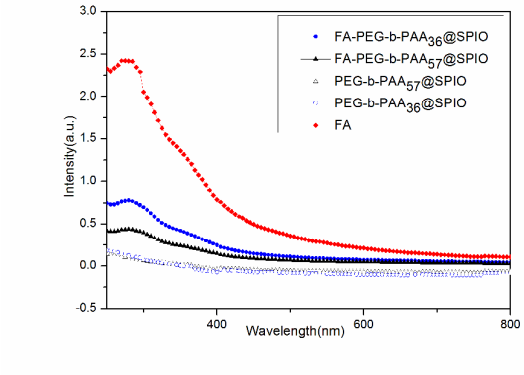

Fig. 5 UV-vis absorption spectra of PEG-b-PAA_{57}@SPION, PEG-b-PAA_{36}@SPION, FA-PEG-b-PAA_{36}@SPION, FA-PEG-b-PAA_{57}@SPION and folic acid in DI water.

3.4 Magnetic properties of PEG-PAA_x@SPION and FA-PEG-PAA_x@SPION

Hysteresis loops measured by vibrating sample magnetometer exhibited similar superparamagnetic characteristics with no remnant magnetization and coercivity of PEG-b-PAA_{36}@SPION and PEG-b-PAA_{57}@SPION as well as folic acid conjugated FA-PEG-b-PAA_{36}@SPION and FA-PEG-b-PAA_{57}@SPION at room temperature (Fig. 6). Based on the TGA results (Fig. S2), the saturation magnetizations (Ms) of PEG-b-PAA_{36}@SPION and PEG-b-PAA_{57}@SPION were calculated to be 54.3 Fe emu/g and 17.0 Fe emu/g respectively, and the Ms for FA-PEG-b-PAA_{36}@SPION and FA-PEG-b-PAA_{57}@SPION were 53.1 Fe emu/g and 13.7 Fe emu/g, respectively, which indicated no obvious loss of magnetization per Fe unit after the conjugation of folic acid.

To further assess their magnetic property for MRI application, r_2 relaxivities of the nanoparticles were calculated by measuring the change of the spin–spin relaxation rate (T_2^{-1}) per unit Fe concentration. r_2 of PEG-b-PAA_{36}@SPION and FA-PEG-b-PAA_{36}@SPION were significantly larger than that of PEG-b-PAA_{57}@SPION and FA-PEG-b-PAA_{57}@SPION, whereas conjugation of folic acid possess little impact on the r_2 value of the nanoparticle. Hysteresis loops and r_2 relaxivities results indicated that PEG-b-PAA_{36}@SPION was much more magnetic sensitive than PEG-b-PAA_{57}@SPION. This might be attributed to the larger core size and therefore smaller spin canting effect of PEG-b-PAA_{36}@SPION.[31, 32] r_2 value of FA-PEG-b-PAA_{36}@SPION was close to that of Resovist,[31] a commercial SPION for lymph node imaging which hydrodynamic size is about 40 nm. The reason might lie in the fact that commercial Resovist was obtained by co-precipitation method, while

polyol method produced PEG-b-PAA@SPION were prepared under high temperature condition. Due to the strong ostwald ripening procedure, crystallinity and magnetic performance of the iron oxide was improved.[33, 34]

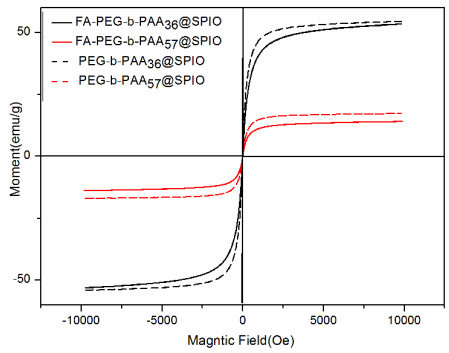

Fig. 6 Magnetization curves of PEG-b-PAA_{36}@SPION, FA-PEG-b-PAA_{36}@SPION, PEG-b-PAA_{57}@SPION and FA- PEG-b-PAA_{57}@SPION.

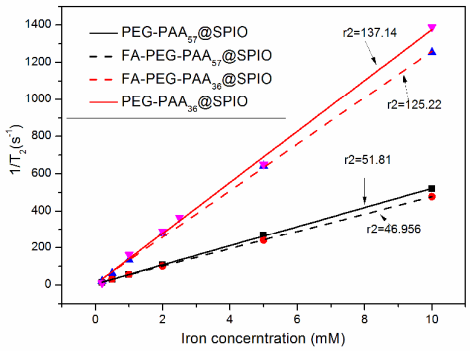

Fig. 7 Plot of r_2 as a function of the iron concentration of PEG-b-PAA_{36}@SPION, FA-PEG-b-PAA_{36}@SPION, PEG-b-PAA_{57}@SPION and FA-PEG-b-PAA_{57}@SPION.

3.5 Specific endocytosis of FA-PEG-b-PAAx@SPION

As folate receptor expression of RAW264.7 cells could be largely up-regulated by activation of IFN-γ/TNF-α.[17] Specificity targeting ability of FA-PEG-PAA@SPION to folate receptor was tested through Prussian blue staining of activated RAW264.7

cells which have endocytosed PEG-b-PAA@SPIO or FA-PEG-b-PAA@SPIO**.** The condition of the cellular endocytosis was optimized by changing the time and concentration of the nanoparticles used (Fig. S4, S5). After that, experiment was conducted to investigate the specific endocytosis of FA-PEG-b-PAA@SPION and PEG-b-PAA@SPION. Fig. 8 indicated that cellular uptake amount of FA-PEG-b-PAA@SPION (blue granules) was more than that of PEG-b-PAA@SPION, which proved the specific targeting ability of folic acid. Moreover, the amount of cellular uptake of FA-PEG-b-PAA_{36}@SPION was obviously larger than that of FA-PEG-b-PAA_{57}@SPION. Iron concentrations of cellular uptake amount were measured by ferrozine assay (Fig. S6) and the results consisted with prussia staining. Cellular uptake amounts of FA-PEG-b-PAA@SPION were two times larger than that of PEG-b-PAA@SPION, while cellular uptake amount of FA-PEG-b-PAA_{36}@SPION was nearly four times larger than that of FA-PEG-b-PAA_{57}@SPION. These results indicated that FA-PEG-b-PAA_{36}@SPION was a preferable SPION for active targeting compared to FA-PEG-b-PAA_{57}@SPION.

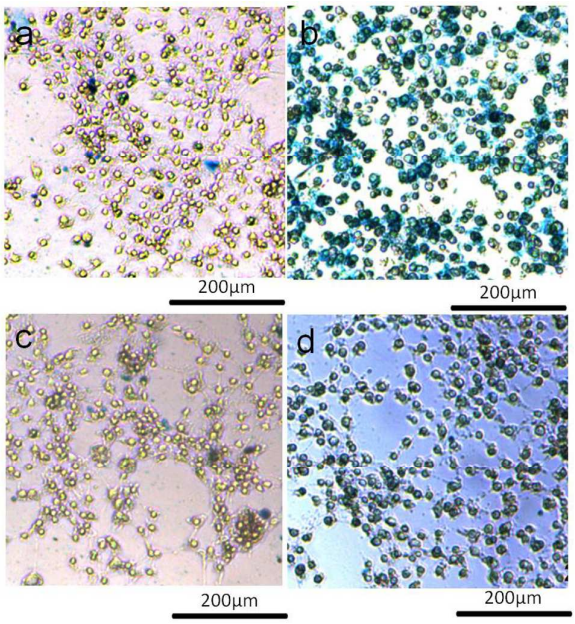

Fig. 8 Prussia staining of RAW264.7 uptake of FA-PEG-b-PAA_{57}@SPION(a), FA-PEG-b-PAA_{36}@SPION (b), PEG-b-PAA_{57}@SPION (c), and PEG-b-PAA_{36}@SPION(d).

3.6 SPION enhanced MRI of Antigen-Induced Arthritis

AIA model was successfully built by intradermal injection of complete Freund's adjuvant at back feet of the rats. Inflammatory cells (arrow) like macrophages could be found in synovium and peripheral area of the arthritic joint in light micrographs of the hematoxylin–eosin stain sample (Fig. S7). Based on magnetic properties test and endocytosis experiment, FA-PEG-b-PAA_{36}@SPION was chosen as the preferable nanoparticle for MRI application of RA joint. Representative T_2-weighted images of the SPION groups using 7T MRI equipment were presented in Fig. 9. Synovium of animals appeared a moderate signal decline on T_2-weighted MR images after intravenous injection of PEG-b-PAA_{36}@SPION (Fig. 9a). This finding indicated that non-specific SPION could passively target the RA joint. In comparison, FA-PEG-b-PAA_{36}@SPION contrasted MRI demonstrated a more intact and clearer

structure of synovium (Fig. 9b), suggesting that SPION were preferentially endocytosed by macrophages in the inflamed synovium. For FA-PEG-b-PAA_{36}@SPION, signal intensity ratio of surrounding water proton / the arrowhead indicated area was 1.410 times larger than that of PEG-b-PAA_{36}@SPION, which indicated the signal decrease of the arrow indicated area contrasted by FA-PEG-b-PAA_{36}@SPION was larger than that of PEG-b-PAA_{36}@SPION. These results suggested that the FA-PEG-b-PAA_{36}@SPION might be useful as a target MRI contrast to qualify the arthritic joint.

To better understand targeting ability and biodistribution of the nanoparticles, ankle joint and major organs including liver, spleen, kidney, heart and lung were harvested and stained by Prussian blue after MRI (Fig. 10). Results indicated that PEG-b-PAA_{36}@SPION could passively accumulate in ankle joint, whereas FA-PEG-b-PAA_{36}@SPION has shown a qualitative better accumulation in the joint, which might be due to the active targeting of folic acid. Except for joint, spleen and lung were found to have a small amount of SPION accumulation, which might be attributed to the macrophages endocytosis of nanoparticles by reticuloendothelial systems,[32, 35] while liver, heart and kidney showed little accumulation of the nanoparticle.

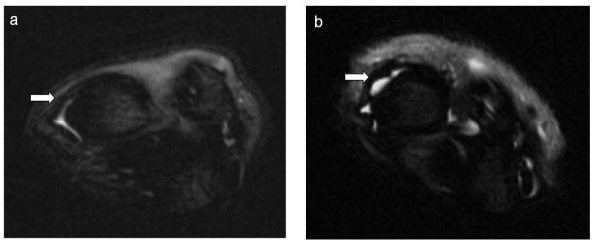

Fig. 9 PEG-b-PAA_{36}@SPION (a) and FA-PEG-b-PAA_{36}@SPION (b) contrast T_2 weighted MRI in

arthritic rat ankle joint24 h after intravenous injected of SPION (arrows indicate the synovium sites).

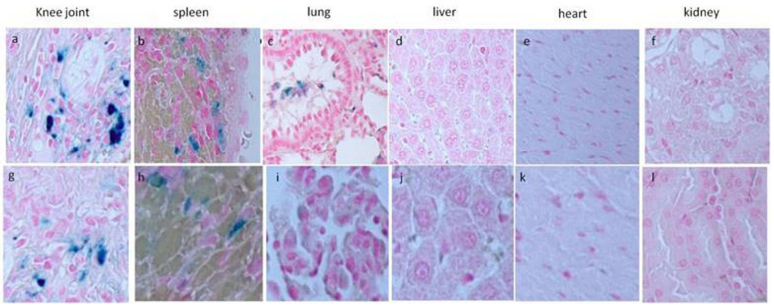

Fig. 10 Prussian blue staining images of major organs including ankle joint (a,g), spleen (b,h), lung (c,i), liver (d,j), heart (e,k) and kidney (f,l) one day after injection of FA-PEG-b-PAA_{36}@SPION (a-f) and PEG-b-PAA_{36}@SPION(g-l) 24 h after intravenous injected of SPION.

Conclusion

In summary, a novel PEG-b-PAA@SPION contrast was synthesized by using an in situ polyol method. Nanoparticles of different sizes were obtained by controlling the chain length of the PAA block of the copolymer PEG-b-PAA_X. By measuring the magnetic sensitivity, colloid stability and specific targeting ability, FA-PEG-b-PAA_{36}@SPION was chosen as contrast agent for MRI of RA joint. Signal of synovium was significantly enhanced in 7T MRI after administration of FA-PEG-b-PAA_{36}@SPION in AIA model rats. Correlated histological outcome of prussia blue staining also confirmed the excellent permeability efficiency of the folic acid conjugated PEG-b-PAA_{36}@SPION in joint. The enhanced MR imaging results proved significant opportunity of FA-PEG-PAA@SPION contrast agent for targeted human diagnosis of rheumatoid arthritis.

Acknowledgements

This work was financially supported by the National Natural Science Foundation of China (Grants NO. 21304099, 51203162, 51103159, 51373177), the National High Technology Research and Development Program (Grants NO. 2014AA020708, 2012AA022703 and 2012AA020804), Instrument Developing Project of the Chinese Academy of Sciences (Grant No. YZ201253, YZ201313), Open Funding Project of the National Key Laboratory of Biochemical Engineering (Grant NO. Y22504A169). "Strategic Priority Research Program" of the Chinese Academy of Sciences，Grant No. XDA09030301-3.

Reference

1. H. K. Choi, M. A. Hernan, J. D. Seeger, J. M. Robins and F. Wolfe, *Lancet*, 2002, **359**, 1173-1177.
2. F. M. McQueen, *Rheumatology*, 2000, **39**, 700-706.
3. G. H. Simon, J. von Vopelius-Feldt, M. F. Wendland, Y. Fu, G. Piontek, J. Schlegel, M. H. Chen and H. E. Daldrup-Link, *J Magn Reson Imaging*, 2006, **23**, 720-727.
4. C. S. Reiner, A. M. Lutz, F. Tschirch, J. M. Froehlich, S. Gaillard, B. Marincek and D. Weishaupt, *European Radiology*, 2009, **19**, 1715-1722.
5. N. Butoescu, C. A. Seemayer, M. Foti, O. Jordan and E. Doelker, *Biomaterials*, 2009, **30**, 1772-1780.
6. A. G. Roca, S. Veintemillas-Verdaguer, M. Port, C. Robic, C. J. Serna and M. P. Morales, *J Phys Chem B*, 2009, **113**, 7033-7039.
7. S. Tong, S. Hou, B. Ren, Z. Zheng and G. Bao, *Nano Letters*, 2011, **11**, 3720-3726.
8. B. J. Dardzinski, G. Boivin, J. Lewis and R. Hirsch, *Arthritis and Rheumatism*, 1999, **42**, S119-S119.
9. S. H. Wang, X. Y. Shi, M. Van Antwerp, Z. Y. Cao, S. D. Swanson, X. D. Bi and J. R. Baker, *Advanced Functional Materials*, 2007, **17**, 3043-3050.
10. X. Y. Shi, S. H. Wang, S. D. Swanson, S. Ge, Z. Y. Cao, M. E. Van Antwerp, K. J. Landmark and J. R. Baker, *Advanced Materials*, 2008, **20**, 1671-1678.
11. D. F. Liu, W. Wu, J. J. Ling, S. Wen, N. Gu and X. Z. Zhang, *Advanced Functional Materials*, 2011, **21**, 1498-1504.
12. Y. Zhang, N. Kohler and M. Q. Zhang, *Biomaterials*, 2002, **23**, 1553-1561.
13. J. C. Li, L. F. Zheng, H. D. Cai, W. J. Sun, M. W. Shen, G. X. Zhang and X. Y. Shi, *Biomaterials*, 2013, **34**, 8382-8392.
14. C. M. Paulos, M. J. Turk, G. J. Breur and P. S. Low, *Advanced Drug Delivery Reviews*, 2004, **56**,

1205-1217.

15. M. A. Guo, C. L. Que, C. H. Wang, X. Z. Liu, H. S. Yan and K. L. Liu, *Biomaterials*, 2011, **32**, 185-194.
16. F. Sonvico, S. Mornet, S. Vasseur, C. Dubernet, D. Jaillard, J. Degrouard, J. Hoebeke, E. Duguet, P. Colombo and P. Couvreur, *Bioconjugate Chemistry*, 2005, **16**, 1181-1188.
17. F. Schmitt, L. Lagopoulos, P. Kauper, N. Rossi, N. Busso, J. Barge, G. Wagnieres, C. Laue, C. Wandrey and L. Juillerat-Jeanneret, *Journal of Controlled Release*, 2010, **144**, 242-250.
18. X. Cai, H. Zhou, Y. F. Wong, Y. Xie, Z. Q. Liu, Z. H. Jiang, Z. X. Bian, H. X. Xu and L. Liu, *Biochemical and Biophysical Research Communications*, 2005, **337**, 586-594.
19. L. E. W. LaConte, N. Nitin, O. Zurkiya, D. Caruntu, C. J. O'Connor, X. Hu and G. Bao, *Journal of Magnetic Resonance Imaging*, 2007, **26**, 1634-1641.
20. A. M. Mohs, Y. D. Zong, J. Y. Guo, D. L. Parker and Z. R. Lu, *Biomacromolecules*, 2005, **6**, 2305-2311.
21. H. F. Xu, F. H. Meng and Z. Y. Zhong, *Journal of Materials Chemistry*, 2009, **19**, 4183-4190.
22. Y. P. Wang, M. Zhang, C. Moers, S. L. Chen, H. P. Xu, Z. Q. Wang, X. Zhang and Z. B. Li, *Polymer*, 2009, **50**, 4821-4828.
23. K. Xu, Y. Wang, Y. X. Wang, T. Yu, L. J. An, C. Y. Pan and R. Bai, *Polymer*, 2006, **47**, 4480-4484.
24. B. L. Wang, R. J. Ma, G. Liu, X. J. Liu, Y. H. Gao, J. Y. Shen, Y. L. An and L. Q. Shi, *Macromolecular Rapid Communications*, 2010, **31**, 1628-1634.
25. C. M. Cheng, F. J. Xu and H. C. Gu, *New Journal of Chemistry*, 2011, **35**, 1072-1079.
26. S. Lefevre, D. Ruimy, F. Jehl, A. Neuville, P. Robert, C. Sordet, M. Ehlinger, J. L. Dietemann and G. Bierry, *Radiology*, 2011, **258**, 722-728.
27. S. C. Wuang, K. G. Neoh, E. T. Kang, D. W. Pack and D. E. Leckband, *Journal of Materials Chemistry*, 2007, **17**, 3354-3362.
28. C. Huang, K. G. Neoh and E.-T. Kang, *Langmuir*, 2011, **28**, 563-571.
29. X. Y. Shi, T. P. Thomas, L. A. Myc, A. Kotlyar and J. R. Baker, *Physical Chemistry Chemical Physics*, 2007, **9**, 5712-5720.
30. J. H. Maeng, D.-H. Lee, K. H. Jung, Y.-H. Bae, I.-S. Park, S. Jeong, Y.-S. Jeon, C.-K. Shim, W. Kim, J. Kim, J. Lee, Y.-M. Lee, J.-H. Kim, W.-H. Kim and S.-S. Hong, *Biomaterials*, 2010, **31**, 4995-5006.
31. S. Laurent, D. Forge, M. Port, A. Roch, C. Robic, L. Vander Elst and R. N. Muller, *Chem Rev*, 2008, **108**, 2064-2110.
32. E. D. Smolensky, H. Y. E. Park, Y. Zhou, G. A. Rolla, M. Marjanska, M. Botta and V. C. Pierre, *Journal of Materials Chemistry B*, 2013, **1**, 2818-2828.
33. M. V. Kovalenko, M. I. Bodnarchuk, R. T. Lechner, G. Hesser, F. Schaffler and W. Heiss, *Journal of the American Chemical Society*, 2007, **129**, 6352-6353.
34. X. W. Teng and H. Yang, *Journal of Materials Chemistry*, 2004, **14**, 774-779.
35. Y. M. Liu, K. Yang, L. Cheng, J. Zhu, X. X. Ma, H. Xu, Y. G. Li, L. Guo, H. W. Gu and Z. Liu, *Nanomedicine-Nanotechnology Biology and Medicine*, 2013, **9**, 1077-1088.